# Optimal prestressing of triple-bay prestressed stayed columns

Jialiang Yu, M. Ahmer Wadee*

*Department of Civil and Environmental Engineering, Imperial College London, South Kensington Campus, London SW7 2AZ, UK*

**Abstract**

A nonlinear finite element model of a triple-bay prestressed stayed column is developed within the commercial package ABAQUS. A linearly obtained 'optimal prestressing force' that maximizes the critical buckling load is investigated since this quantity has been demonstrated in previous work on single-bay prestressed columns to provide a lower bound to the actual maximum load carrying capacity when compared to experimental results and nonlinear modelling. The ratio of the crossarm to the overall column length, the diameter of the cable stays, the relative lengths of the individual crossarms and the ratio of the initial prestressing force to the aforementioned linear optimal prestress are varied. Measures for the relative efficiency of the main column and the stays are defined and the objective of the optimization study is for the efficiency to be maximized. It is found that the true optimal prestress is generally higher than the equivalent, linearly obtained, quantity but by a significantly reduced factor when compared to an equivalent study for single-bay prestressed stayed columns.

*Keywords:* Finite element modelling; Stability; Post-buckling; Prestress; Interactive buckling; Optimization

## 1. Introduction

Prestressed stayed columns, which are usually made from tubular steel elements that are reinforced by external cable stays, as represented in Figure 1, are being increasingly used in the construction industry. With the introduction of the crossarms and prestressed cables, stayed columns possess significant extra axial strength when compared with conventional columns without necessarily a commensurate increase in self-weight. This type of structure offers an innovative, aesthetic and practical solution to the problem of low critical buckling load capacities in highly slender columns. For example, during the construction of the Rock in Rio III stadium in Brazil [1, 2], such columns were used as a lightweight solution to prop the incomplete stadium roof while the construction was completed. The columns were

*Corresponding author

*Email addresses:* j.yu12@imperial.ac.uk (Jialiang Yu), a.wadee@imperial.ac.uk (M. Ahmer Wadee)

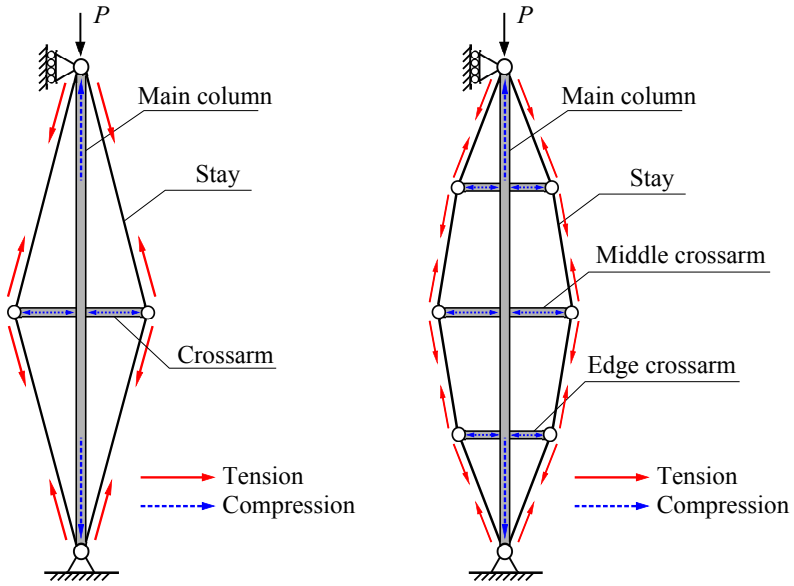


(a) Single-bay column (b) Triple-bay column

Figure 1: Columns reinforced by cable stays with different crossarm systems.

constructed and prestressed on site such that they eliminated the need for using expensive shoring systems that would have increased the time and cost of construction significantly. Figure 2 shows some other real-world applications of prestressed stayed columns with multiple bays.

Research on such structural components can be dated from the 1960s. The initial research focus mainly concerned the evaluation of the critical buckling load [3, 4, 5, 6, 7, 8, 9]. Effects of different levels of prestress [10] and initial imperfections were then studied [11, 12]. The nonlinear behaviour of prestressed stayed columns has only been studied extensively relatively recently [13, 14]. This more recent work has demonstrated that although for each configuration of crossarm length, main column length and stay diameter there exists a so-called 'optimal prestressing force' that maximizes the critical buckling load [10], the behaviour of the columns in the post-buckling range is considerably more complex and affects the ultimate load carrying capacity [15, 16, 17, 18, 19]. The work has resulted in recommendations for the actual optimal initial prestress accounting for the post-buckling behaviour and the development of a detailed procedure for the design of such single-bay column systems [20, 21].

Most existing studies have been focused on single-bay stayed columns while multiple crossarm cases have only been recently investigated in terms of nonlinear behaviour [19]. It has been shown that there is a great deal of advantage to be gained from the introduction of crossarms. However, the benefits can be outweighed by the increased cost by demanding higher structural strengths from the individual elements of the system. Saito and Wadee presented a study of the optimal prestress in terms of the ultimate strength and cost effectiveness for the single-bay column [20] and determined the recommended prestress

(a) Chiswick Park, London, UK

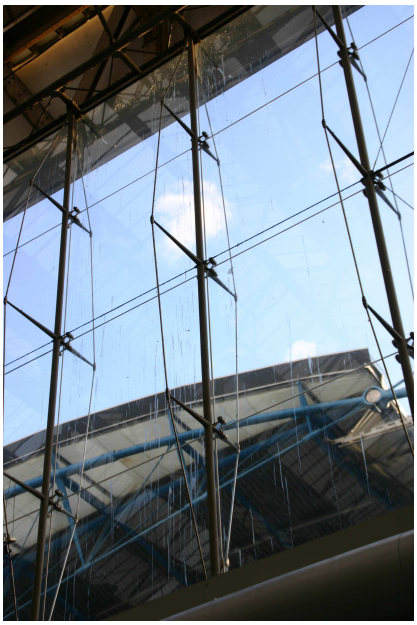

(b) London Waterloo Station, UK

(c) Parkland Mall, Dalian, China

Figure 2: Applications of prestressed stayed columns in the construction industry; photographs (a) and (b) were taken by Daisuke Saito; photograph (c) was taken by the lead author.

values. Unlike earlier research on the magnitude of the prestress [22], the maximum load carrying capacity is not necessarily the only indicator for choosing the preferred level of prestress. The required resistances of the column and the stays need also to be taken into consideration. This allows the designer to choose the appropriate prestress level more wisely when designing the stayed column, since the strength of the materials and their relative costs are also important factors. A similar approach is also used in the current study to investigate the actual optimal prestress for the triple-bay prestressed stayed column. Recommendations for the actual optimal prestress are provided for the structures with different geometric arrangements.

## 2. Model formulation

The model of the triple-bay prestressed stayed column is formulated by using the commercial finite element (FE) software ABAQUS [23]. It comprises a main column element, three pairs of crossarms and a series of prestressed cable stays. Since the main column element is very slender, it is modelled using 'B23' cubic Euler–Bernoulli beam elements, whereas the generally shorter crossarms are modelled using the 'B22' quadratic Timoshenko beam elements such that the effects of flexural shear may be captured. The stays are modelled with the 'T2D2' truss elements with the 'no compression' option enabled to ensure the stays only resist tension [24]. Moreover, the stay components are modelled as separate finite elements to enable each component to carry different forces, which has been

demonsrated to simulate the mechanical problem accurately [14, 25]. As shown in Figure 3(a), the stayed column is simply-supported and loaded axially. Three pairs of crossarms

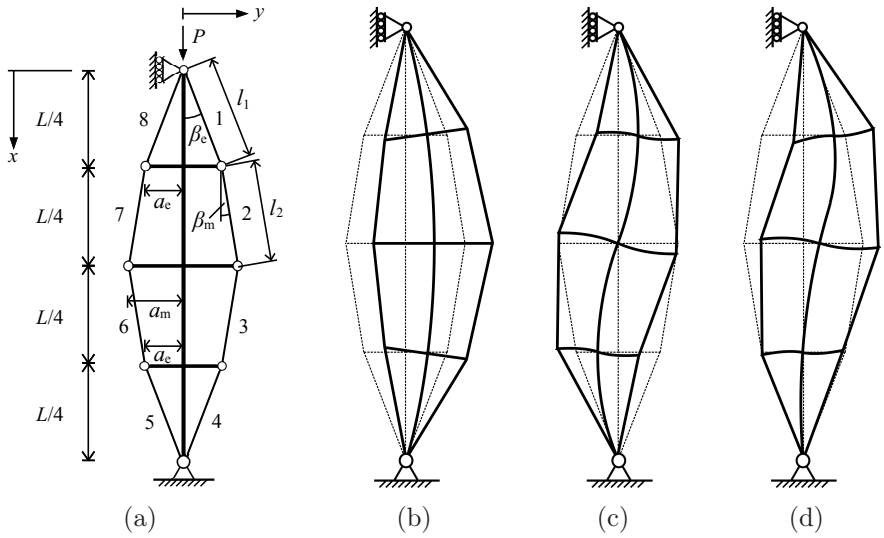


Figure 3: (a) The simply-supported triple-bay prestressed stayed column with geometric and stay component number definitions (1–8 inclusive); (b) symmetric buckling Mode 1; (c) antisymmetric buckling Mode 2; (d) interactive post-buckling profile.

are rigidly connected to the one-quarter, one-half and three quarter length points of the main column. Prestressed cable stays are assumed to be pinned to the ends of the column and the tips of the crossarms. The length ratio of the edge crossarm to the middle crossarm is defined as $\gamma = a_e/a_m$ and is one of the key parameters varied in the current study since it has been shown to have a significant impact on the effectiveness of the system [26].

Different arrangements of crossarms along the length in the $yz$-plane may be used, as shown in Figure 4 with (a) showing the simplest one-dimensional system with both (b)

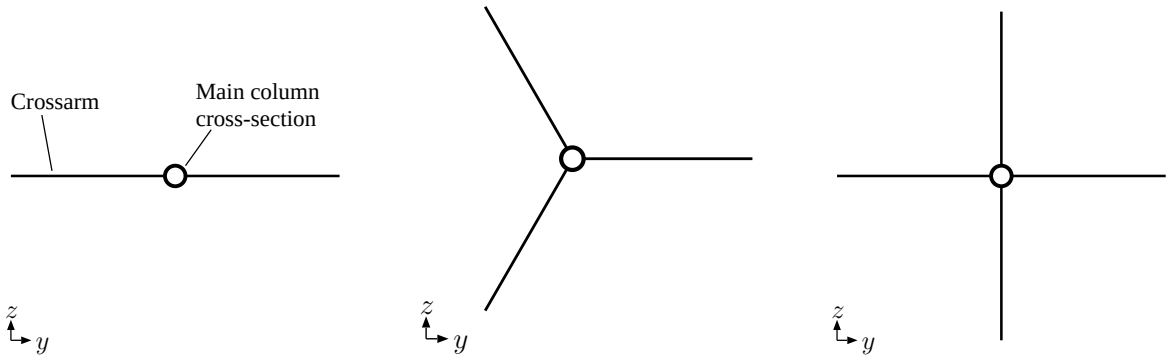


Figure 4: Different numbers of branches in each crossarm system along the length. Case (a) is only practical if buckling displacements are constrained to be purely in the $y$-direction; cases (b) and (c) would work if the column displaces anywhere in the $yz$-plane.

and (c) showing two-dimensional systems. Note that the column in practice should be supported by at least three crossarms in the $yz$-plane. This would ensure that it would benefit from the increased load carrying capacity by avoiding an obviously weaker buckling axis, assuming that the main column element is either a circular or square hollow section. The single-bay case with a three crossarm rosette, as represented in Figure 4(b), was studied recently in [27] and as a potential unit cell in a lattice material [28]. Currently, the triple-bay system is assumed to have either the case shown in Figure 4(a) with deflections in the $z$-direction completely restrained or, effectively, the case shown in Figure 4(c) where it has been demonstrated previously that the system has no preferred buckling direction [29]. These two respective cases are also represented in the photographs shown in Figures 2(b) and 2(c) in turn. Hence, a two-dimensional model in the $xy$-plane, as depicted in Figure 3(a), is studied currently since it is simple yet practical. Finally, it should be noted that the FE model implemented currently has been validated both for the linear and nonlinear ranges in a recent study [19].

### *2.1. Benchmark prestress*

An initial prestressing force is applied to the cable stays in order to increase the load carrying capacity. The optimal initial prestressing force $T_{\text{opt}}$ that maximizes the critical buckling load ($P^{\text{C}}_{\text{max}}$) for the single-bay stayed column was presented by Hafez *et al* [10], as shown in Figure 5, which shows a representation of the relationship between the critical

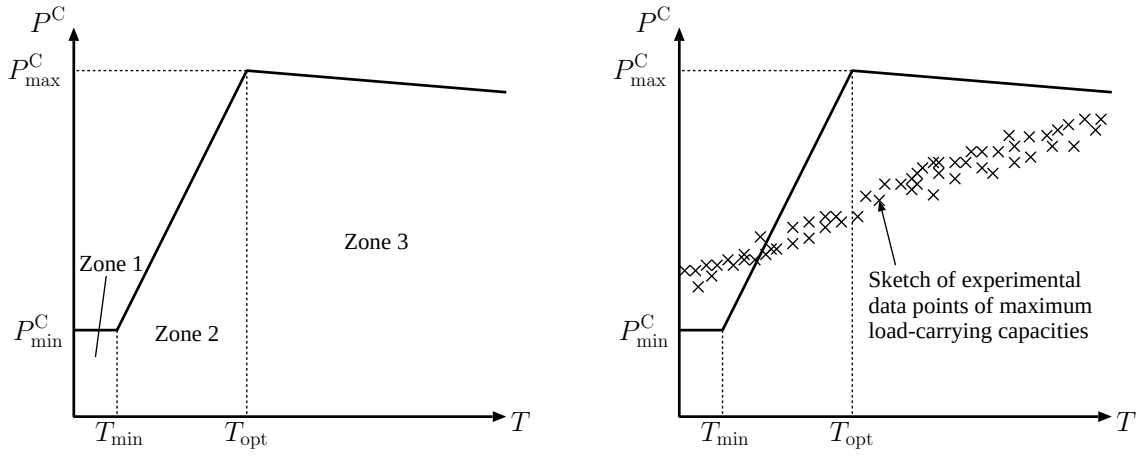


Figure 5: Critical buckling load $P^{\text{C}}$ versus initial prestressing force $T$ with (left) the zone distinction determined by Hafez *et al* [10] and (right) the actual ultimate strengths of single-bay stayed columns from experiments superimposed on the same graph determined by Temple [12].

buckling load and the initial prestress in the column. Zone 1 represents a very small prestress that would completely disappear under increasing axial loading before or at the instant when the classical Euler buckling load of the unstayed column is reached; effectively that structure would be identical to the unstayed column. The prestress in Zone 2 is sufficiently large to make the buckling load of the column larger than the Euler load, but

the column buckles immediately once the prestress disappears from the stays. The prestress in Zone 3 is even larger, as a result there are residual forces in the stays when the column buckles. The vertical components of the residual force in the stays effectively become a part of the applied force, which leads to a decrease in the buckling load with the increase of the initial prestress. Hafez *et al.* indicated that the prestress at the intersection of Zones 2 and 3 were the desired optimal prestress, the objective of their study being to maximize the linear critical buckling load with respect to the initially introduced prestressing force within the stays. By a similar, but slightly extended, calculation for the triple-bay stayed column, an expression for the optimal initial prestressing force $T_{\text{opt}}$ can be expressed thus [19, 24]:

$$T_{\text{opt}} = P^{\text{C}} \frac{C_{11}}{C_{22}}, \tag{1}$$

where:

$$\begin{aligned} C_{11} &= \frac{\cos\beta_{\text{m}}}{2K_{\text{c}}\left[\dfrac{2}{K_{\text{s2}}} + \dfrac{\cos^2\beta_{\text{m}}}{K_{\text{c}}} + \dfrac{4\sin^2\beta_{\text{m}} + 2\gamma(\sin\beta_{\text{e}}\sin\beta_{\text{m}} - \sin^2\beta_{\text{m}})}{K_{\text{m}}}\right]}, \\ C_{22} &= 1 + \frac{\cos\beta_{\text{e}}\cos\beta_{\text{m}}}{2K_{\text{c}}\left[\dfrac{1}{K_{\text{s2}}} + \dfrac{2\sin^2\beta_{\text{m}} + \gamma(\sin\beta_{\text{e}}\sin\beta_{\text{m}} - \sin^2\beta_{\text{m}})}{K_{\text{m}}}\right]}, \end{aligned} \tag{2}$$

where $K_{\text{c}}$, $K_{\text{m}}$ and $K_{\text{s2}}$ are the axial stiffnesses of the main column, the middle crossarm and stay number 2 respectively, thus:

$$K_{\text{c}} = \frac{E_{\text{c}}A_{\text{c}}}{L}, \quad K_{\text{m}} = \frac{E_{\text{a}}A_{\text{a}}}{a_{\text{m}}}, \quad K_{\text{s2}} = \frac{E_{\text{s}}A_{\text{s}}}{l_2}, \tag{3}$$

with $E_{\text{c}}$, $E_{\text{a}}$ and $E_{\text{s}}$ being the Young's Moduli alongside $A_{\text{c}}$, $A_{\text{a}}$ and $A_{\text{s}}$ being the cross-sectional areas of the main column, the crossarm and the stays respectively. The length of stay 2, $l_2$, is $\sqrt{(a_{\text{m}} - a_{\text{e}})^2 + L^2/16}$. The critical buckling load $P^{\text{C}}$ is evaluated from linear eigenvalue analysis without the consideration of the initial prestressing force, a procedure that has been successfully applied previously [15]. Note that the optimal initial prestressing force $T_{\text{opt}}$ is used as a benchmark in the current study since it is derived from a model that does not take any geometrically nonlinear behaviour into account. It has also been found previously that the ultimate response of the stayed column system is more complex and that the actual failure loads of such systems are in fact maximized at initial prestressing levels that are above and beyond $T = T_{\text{opt}}$ [12], as represented in the right-hand graph of Figure 5. Indeed, a previous study on the actual optimal initial prestressing force for the single-bay column case [20] confirmed that the initial prestressing force should be considerably larger than the value obtained by linear analysis ($T_{\text{opt}}$). Therefore, the determination of the level of the actual optimal initial prestressing force for the triple-bay column is the primary concern in the current work.

*2.2. Geometric imperfections*

Geometric imperfections in the structure of course exist in reality and they are thus taken into consideration presently. As stated earlier, the symmetric and the anti-symmetric buckling modes of the column and their combinations, the latter modelling the asymmetric interactive post-buckling profile, are considered in this study, as shown in Figure 3(b–d). Therefore, a combination of the expressions for Modes 1 and 2, with corresponding scale factors, should be used to ensure interactive buckling is also included. To ensure that imperfections of commensurate magnitude may be compared regardless of the detailed shape of the initial imperfections the induced main column end-shortening $\mathcal{E}_0$ from the imposed imperfection is fixed [30, 31, 32]. The leading order approximation for $\mathcal{E}_0$ is given by the following expression:

$$\mathcal{E}_0 = \int_0^L \frac{1}{2}\big[W_1'^2(x) + W_2'^2(x)\big]\mathrm{d}x, \tag{4}$$

where:

$$W_1(x) = \delta L \mu_1 \sin\frac{\pi x}{L}, \quad W_2(x) = \delta L \mu_2 \sin\frac{2\pi x}{L}. \tag{5}$$

In the expression for $\mathcal{E}_0$, $W_1(x)$ and $W_2(x)$ are shape functions affine to the symmetric mode (Mode 1) and the anti-symmetric mode (Mode 2) of the column, $\delta$ is the normalized amplitude of the initial out-of-straightness of the column. Moreover, $\mu_1$ and $\mu_2$ are the scale factors for the imperfection comprising two modes, representing the contribution of the two distinct modes to the overall buckling shape. To ensure a fair comparison between the results, the end-shortening of the main column element introduced by the imperfection shape is defined to be the same when triggering pure Mode 1, pure Mode 2 or interactive buckling. This procedure ensures that a unique length scale is utilized as the measure of the imperfection size that accounts for both wavelength and amplitude; the common practice of using purely a lateral displacement amplitude tends to bias the results to modes with smaller wavelengths. By substituting $W_1$ and $W_2$ into Equation (4), the following condition is obtained in terms of the scale factors $\mu_i$ that would ensure a combination of $W_1$ and $W_2$ that would give a constant value of $\mathcal{E}_0$ for a given value of $\delta$ [15]:

$$\mu_1^2 + 4\mu_2^2 = 1. \tag{6}$$

The selection of $\mu_1$ and $\mu_2$ shown in Table 1 represents the contribution that each distinct

Table 1: Selected combinations of scale factors $\mu_1$ and $\mu_2$.

| Buckling type | $\mu_1$ | $\mu_2$ |
|---|---|---|
| Mode 1 | 1.000 | 0.000 |
| Interactive | 0.500 | 0.433 |
| Mode 2 | 0.000 | 0.500 |

mode makes to the initial imperfection used to trigger each type of post-buckling profile. Apart from pure Modes 1 and 2 where $\mu_2 = 0$ and $\mu_1 = 0$ respectively, $\mu_1 = 0.5$ is used

to represent interactive buckling, the specified combination of the two pure modes. Unless stated otherwise, the generic imperfection size $\delta$ is 1/300, which represents the EC3 design value for hot rolled sections [33], is used throughout the current work. This value effectively accounts for both initial geometric deformations and residual stresses.

*2.3. Efficiency indicators for the main column and the stays*

It has been observed on several occasions that a larger load carrying capacity of the triple-bay prestressed stayed column can be achieved by increasing the initial prestressing force in the stays from the linearly obtained benchmark level $T_{\text{opt}}$ [19, 26]. However, the benefit in the increasing load carrying capacity cannot be obtained in perpetuity by continuing to raise the initial level of the prestress. The larger the prestress in the stays, the larger would be the induced axial stress within the column before external loading is commenced. In cases that have been studied hitherto, although the prestress introduces an extra axial component to the column stress, which very slightly reduces the external load carrying capacity, the extra lateral stiffness that is introduced to the system plays a significantly more important role in resisting the buckling deformation—this essentially neutralizes the potential disadvantage. Therefore, an increase in the load carrying capacity is usually observed. However, if the prestress in the stays is sufficiently large, the effect of the initial axial stress in the column may in fact neutralize the benefit of the extra stiffness in the stays instead—if this were to be the case, the load carrying capacity would begin to decrease for larger initial prestressing forces. Figure 6 shows the relationship of

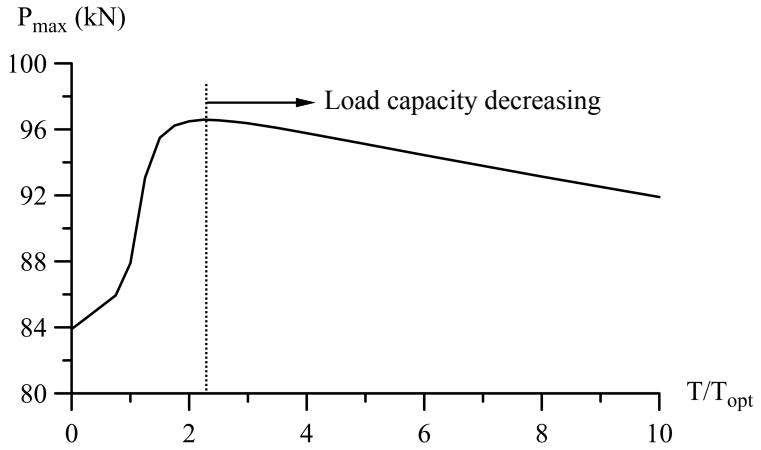


Figure 6: Relationship of the load carrying capacity $P_{\text{max}}$ obtained from the FE model versus the normalized initial prestressing force in the stays $T/T_{\text{opt}}$ for the triple-bay prestressed stayed column with the stay diameter $\phi_{\text{s}} = 4.8$ mm, the column aspect ratio $2a_{\text{m}}/L = 0.2$ and the crossarm ratio $\gamma = a_{\text{e}}/a_{\text{m}} = 0.8$.

the load carrying capacity $P_{\text{max}}$ obtained from the FE model versus the normalized initial prestressing force in the stays $T/T_{\text{opt}}$ for the triple-bay prestressed stayed column described in Table 2. The normalized slenderness of the main column element $\bar{\lambda}$ is defined by the well known expression [34]:

$$\bar{\lambda} = \sqrt{P_{\text{y}}/P_{\text{E}}}, \tag{7}$$

Table 2: Material properties and structural dimensions of the triple-bay prestressed stayed columns in the numerical study.

| | |
|---|---|
| Young's moduli of the main column and crossarms | $E_{\mathrm{c}} = E_{\mathrm{a}} = 201$ kN/mm$^2$ |
| Young's modulus of the stays | $E_{\mathrm{s}} = 202$ kN/mm$^2$ |
| Outside diameters of the main column and crossarms | $\phi_{\mathrm{co}} = \phi_{\mathrm{ao}} = 38.1$ mm |
| Inside diameters of the main column and crossarms | $\phi_{\mathrm{ci}} = \phi_{\mathrm{ai}} = 25.4$ mm |
| Length of the main column | $L = 5080$ mm |
| Yield stress of the main column and crossarm | $f_{\mathrm{y}} = 355$ N/mm$^2$ |
| Euler buckling load of the main column | $P_{\mathrm{E}} = 6.38$ kN |
| Squash load of the main column | $P_{\mathrm{y}} = 225$ kN |
| Normalized slenderness of the main column | $\bar{\lambda} = 5.94$ |

with $P_{\mathrm{y}}$ being the squash load and $P_{\mathrm{E}}$ being the Euler buckling load of the main column element, where:

$$P_{\mathrm{y}} = A_{\mathrm{c}} f_{\mathrm{y}}, \quad P_{\mathrm{E}} = \frac{\pi^2 E_{\mathrm{c}} I_{\mathrm{c}}}{L^2}, \tag{8}$$

and $I_{\mathrm{c}}$ is the second moment of area of the main column element about the axis of buckling. It can be seen that the load carrying capacity reaches a plateau when the initial prestressing force is approximately $2T_{\mathrm{opt}}$. As expected, by increasing the initial prestressing force further from approximately $2.5T_{\mathrm{opt}}$, a reduction in the load carrying capacity is observed. It would therefore be unwise to use a very large prestress without further investigation. In addition, an excessive initial prestress may also result in the stress in the main column or the stays exceeding the yield stress of those elements. In an imperfect system, particularly with a realistic column initial out-of-straightness value, geometric nonlinearity becomes important at the instant the column is loaded axially. Owing to the lateral deflection of the column, the stays on the convex side of the column will be stretched further. Therefore, before, or at the point of maximum load, the stresses in these stays may already be larger than the material yield stress. If this were to be the case, material damage in the stays would occur and may compromise the stability of the entire system, which implies that the desired design capacity probably would not be achieved. Therefore, apart from the load carrying capacity, the required stay resistance is also an essential factor when investigating an optimal prestress level. It is worth emphasizing that the size of the crossarm element cross-section is currently taken as being identical to the main column element cross-section. This is to simplify the optimization study and to take any potential overstressing of the crossarms out of the current consideration. Of course, smaller crossarm cross-sections are frequently used (see Figure 2) and the inclusion of their consideration and effects on the optimal prestress is left for future work.

The stresses within the column also need to be monitored. As presented in Figure 7, the total stress in the main column element is a combination of the stress from axial compression and from induced bending; the latter being derived from so-called second order effects, the sources of which are the initial imperfections within the main column being amplified under external loading. Although it has been demonstrated that the maximum load carrying capacity is always less than one-half of the column squash load, the effect of

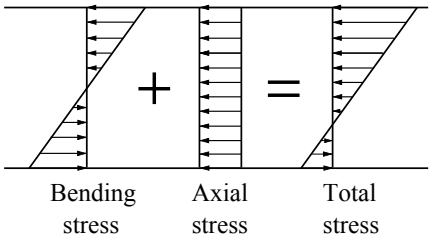


Figure 7: Components of the total direct stresses in the main column element while in the elastic range.

the bending stress has not been studied explicitly. Therefore the effect of both the axial and the bending stresses are investigated currently to ensure that the total direct stress remains within the elastic range throughout the main column cross-section.

Figure 8 shows the stress distribution along the column length at the point of the max-

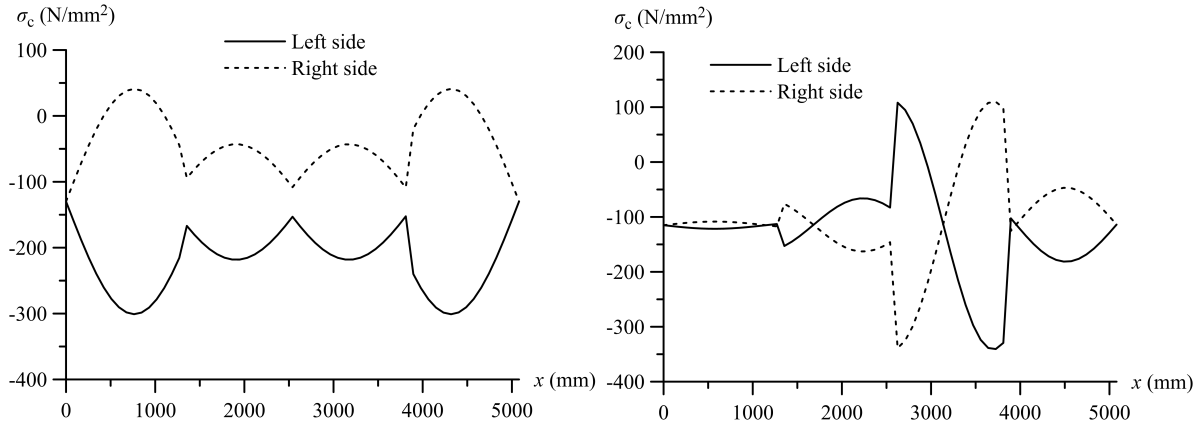


(a) Mode 1 buckling (b) Interactive buckling

Figure 8: Direct stress distribution $\sigma_c$ within the main column element along its length in the post-buckling range for (a) pure Mode 1 and (b) asymmetric interactive buckling where $\phi_s = 4.8$ mm, $2\alpha_m = 0.2$ and $\gamma = 0.8$.

imum load for Mode 1 and interactive buckling when $\phi_s = 4.8$ mm, $2\alpha_m = 0.2$ and $\gamma = 0.8$, where a positive stress value represents tension. As shown in Figure 8(a), in the symmetric buckling (Mode 1) case, the maximum total stress in the column is approximately 300 N/mm$^2$, while the component from the axial load is only approximately 130 N/mm$^2$. This means that the bending stress in this particular location is approximately 170 N/mm$^2$, which is significantly larger than the axial stress. A similar observation can be made from Figure 8(b), which represents interactive buckling; the maximum total stress in the column is approximately 340 N/mm$^2$ while the axial stress is only approximately 115 N/mm$^2$. Again, the bending stress, which is approximately 225 N/mm$^2$, is significantly larger than the axial stress. Therefore, judging whether the column strength is sufficient cannot be accomplished simply by only comparing the axial load capacity with the column squash load [29].

A higher load carrying capacity is almost always preferable. However, extra caution needs to be exercised such that material failure does not occur prior to the failure due to the geometry. Therefore, 'efficiency indicators', first adopted in the study of the single-bay column [20], are used in the current study. Firstly, the efficiency indicator for the main column element is defined thus:

$$\eta_{\mathrm{c}} = \frac{P_{\max}}{A_{\mathrm{c}} f_{\mathrm{y,req}}}, \tag{9}$$

where $P_{\max}$ is the maximum load carrying capacity with $f_{\mathrm{y,req}}$ being the required column resistance at the point of maximum load. A high value of this indicator $\eta_{\mathrm{c}}$ means a relatively high load carrying capacity with an intrinsically low column resistance requirement, which represents a more efficient system. Similarly, the efficiency indicator for the stays is defined thus:

$$\eta_{\mathrm{s}} = \frac{P_{\max}}{A_{\mathrm{s}} f_{\mathrm{s,req}}} \left( \frac{L}{4l_1} \right), \tag{10}$$

where $f_{\mathrm{s,req}}$ is the required stay resistance at the point of the maximum load; the ratio $L/(4l_1)$ is a correction factor, since $l_1$ changes with different values of the column aspect ratio $2\alpha_{\mathrm{m}}$ and the crossarm length ratio $\gamma$, as shown in Figure 3(a). Again, a high value of this indicator $\eta_{\mathrm{s}}$ implies a relatively high load carrying capacity with the stays having a relatively low strength requirement, which represents a more efficient stay system. Therefore, aiming for large values of the two efficiency indicators, $\eta_{\mathrm{c}}$ and $\eta_{\mathrm{s}}$ for the column and the stays respectively, is the objective when investigating the actual optimal prestress currently.

## 3. Results and discussion

To conduct the parametric study, the material and geometric properties that are fixed are presented in Table 2, the numerical values of which are primarily based on previous studies [10, 13, 26, 19]. The study focuses on three parameters: the stay diameter $\phi_{\mathrm{s}}$, the column aspect ratio $2\alpha_{\mathrm{m}}$, where $\alpha_{\mathrm{m}} = a_{\mathrm{m}}/L$, and the length ratio of the edge to the middle crossarm $\gamma = a_{\mathrm{e}}/a_{\mathrm{m}}$. When the model is investigated with $\phi_{\mathrm{s}}$ varying, $2\alpha_{\mathrm{m}}$ is fixed to 0.2 and $\gamma$ is fixed to 0.8. Conversely, when varying $2\alpha_{\mathrm{m}}$, $\phi_{\mathrm{s}}$ is fixed to 4.8 mm and $\gamma$ is fixed to 0.8; when varying $\gamma$, $\phi_{\mathrm{s}}$ is fixed to 4.8 mm and $2\alpha_{\mathrm{m}}$ is fixed to 0.2. The numerical values of the different cases varying $\phi_{\mathrm{s}}$, $2\alpha_{\mathrm{m}}$ and $\gamma$ are listed in Table 3.

### *3.1. Linear buckling analysis*

Buckling analysis in ABAQUS determines the linear eigenvalues and eigenvectors of critical equilibrium modes. The stays are modelled and taken into consideration in the buckling analysis although the prestress $T$ is not introduced at that stage. The buckling loads obtained can then be used to calculate the theoretical optimal prestress using Equation (1), while the eigenvectors are used as the initial imperfections in the main column geometry for the post-buckling analysis, as described in §2.2.

Figure 9 shows the buckling loads from linear eigenvalue analysis of the stayed column with the stay diameter $\phi_{\mathrm{s}}$, the column aspect ratio $2\alpha_{\mathrm{m}}$ and the crossarm length ratio

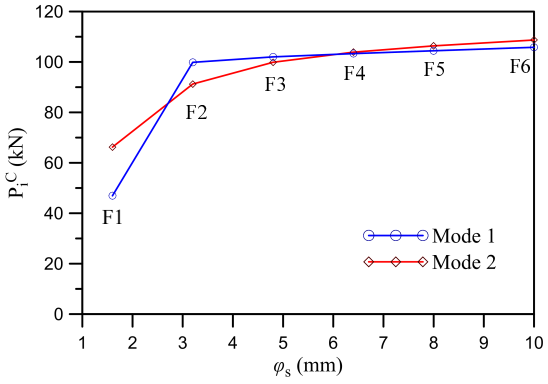


(a) Stay diameter $\phi_s$ varying.

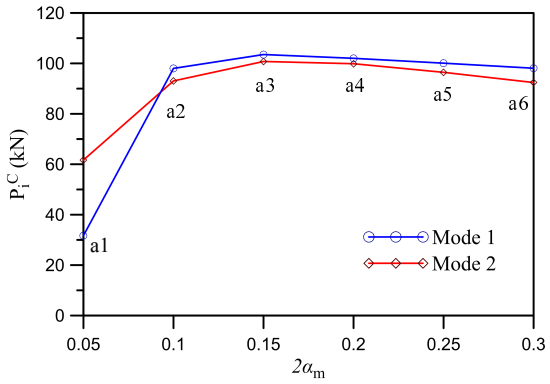


(b) Column aspect ratio $2\alpha_m$ varying.

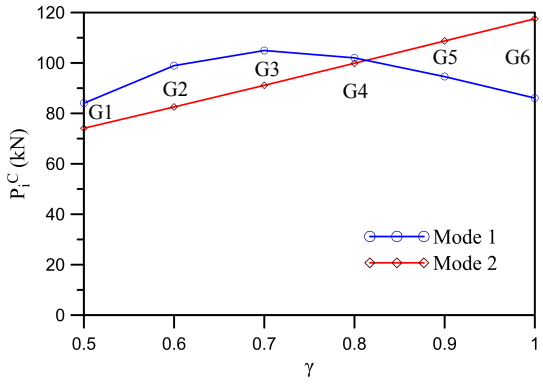


(c) Crossarm length ratio $\gamma$ varying

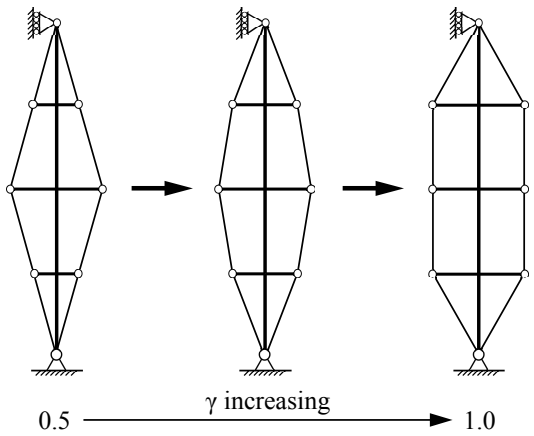


(d) Geometry changes with $\gamma$ varying

Figure 9: Buckling loads of the stayed column with variation of (a) stay diameter $\phi_s$ (cases F1–F6), (b) column aspect ratio $2\alpha_m$ (cases a1–a6) and (c) crossarm length ratio $\gamma$ (cases G1–G6); (d) shows how stayed column geometry changes with $\gamma$.

Table 3: Cases from varying stay diameter $\phi_s$ (where $2\alpha_m = 0.2$ and $\gamma = 0.8$), column aspect ratio $2\alpha_m$ (where $\phi_s = 4.8$ mm and $\gamma = 0.8$) and crossarm length ratio $\gamma$ (where $\phi_s = 4.8$ mm and $2\alpha_m = 0.2$).

| Case | F1 | F2 | F3 | F4 | F5 | F6 |
|---|---|---|---|---|---|---|
| $\phi_s$ (mm) | 1.6 | 3.2 | 4.8 | 6.4 | 8.0 | 10.0 |
| | | | | | | |
| Case | a1 | a2 | a3 | a4 | a5 | a6 |
| $2\alpha_m$ | 0.05 | 0.10 | 0.15 | 0.20 | 0.25 | 0.30 |
| | | | | | | |
| Case | G1 | G2 | G3 | G4 | G5 | G6 |
| $\gamma$ | 0.5 | 0.6 | 0.7 | 0.8 | 0.9 | 1.0 |

$\gamma$ varying. First of all, it should be noted that in almost all the cases considered, the critical buckling loads obtained are an order of magnitude higher than the buckling load of the unstayed column $P_E$, demonstrating the effectiveness of the stayed column system. Moreover, it can be seen in Figure 9(a) that, when the stay diameter $\phi_s$ is relatively small, Mode 1 is critical. Along with the increase of the stay diameter, the buckling loads of Modes 1 and 2 become closer together. Mode 2 becomes critical when the stay diameter $\phi_s$ is increased to 3.2 mm and keeps governing until the stay diameter is 6.4 mm, when Mode 1 becomes critical once again. Similarly, Figure 9(b) indicates that when the column aspect ratio, which is represented by $2\alpha_m$, is relatively small, Mode 1 is critical. Mode 2 becomes critical when $2\alpha_m$ is increased to 0.1 and continues to govern beyond that point. Figure 9(c) shows the critical buckling loads of the column with $\gamma$ varying. The value $\gamma = 0.5$ indicates that the edge crossarms are exactly half of the length of the middle crossarm, while $\gamma = 1.0$ indicates that all the crossarms have the same length. For the initial case, when the edge crossarm length is shorter, Mode 2 is critical. Along with the increase in $\gamma$, the buckling load of Mode 2 keeps increasing, while the buckling load of Mode 1 increases to a maximum value when $\gamma = 0.7$ and then begins to decrease again. As a result, Mode 1 governs again when $\gamma > 0.8$. It is also important to note that the lowest critical buckling loads occur when $\gamma = 0.5$ and 1.0, indicating that the edge crossarms and the middle crossarm are less effective in those respective cases. The largest critical buckling load can be found when $\gamma = 0.8$, which is the reason why this $\gamma$ value is selected as the benchmark while varying the other parameters. This situation may change if additional stays connected the main column to the midspan crossarm, as shown in the practical case of Figure 2(a), but this consideration is left for future work.

With the derivation of the critical loads for different cases, the theoretical optimal initial prestressing force $T_{opt}$ can be calculated by using the expressions stated earlier. Tables 4, 5 and 6 show the values of the calculated values of $T_{opt}$ for the triple-bay prestressed stayed column with the stay diameter $\phi_s$ (cases F1–F6), the column aspect ratio $2\alpha_m$ (cases a1–a6) and the crossarm length ratio $\gamma$ (cases G1–G6) varying respectively.

Table 4: Optimal initial prestressing force $T_{\text{opt}}$ obtained with stay diameter $\phi_{\text{s}}$ varying.

| Case | $\phi_{\text{s}}$ (mm) | $P_1^{\text{C}}$ (kN) | $P_2^{\text{C}}$ (kN) | Critical mode | $P^{\text{C}}$ (kN) | $T_{\text{opt}}$ (kN) |
|---|---|---|---|---|---|---|
| F1 | 1.6 | 46.93 | 66.24 | 1 | 46.93 | 0.15 |
| F2 | 3.2 | 99.85 | 91.24 | 2 | 91.24 | 1.10 |
| F3 | 4.8 | 102.02 | 99.87 | 2 | 99.87 | 2.56 |
| F4 | 6.4 | 103.31 | 103.88 | 1 | 103.31 | 4.36 |
| F5 | 8.0 | 104.44 | 106.38 | 1 | 104.44 | 6.25 |
| F6 | 10.0 | 105.81 | 108.70 | 1 | 105.81 | 8.58 |

Table 5: Optimal initial prestressing force $T_{\text{opt}}$ obtained with column aspect ratio $2\alpha_{\text{m}}$ varying.

| Case | $2\alpha_{\text{m}}$ | $P_1^{\text{C}}$ (kN) | $P_2^{\text{C}}$ (kN) | Critical mode | $P^{\text{C}}$ (kN) | $T_{\text{opt}}$ (kN) |
|---|---|---|---|---|---|---|
| a1 | 0.05 | 31.71 | 61.68 | 1 | 31.71 | 0.81 |
| a2 | 0.10 | 98.01 | 93.05 | 2 | 93.05 | 2.39 |
| a3 | 0.15 | 103.51 | 100.76 | 2 | 100.76 | 2.59 |
| a4 | 0.20 | 102.02 | 99.87 | 2 | 99.87 | 2.56 |
| a5 | 0.25 | 100.09 | 96.45 | 2 | 96.45 | 2.48 |
| a6 | 0.30 | 98.08 | 92.41 | 2 | 92.41 | 2.37 |

Table 6: Optimal initial prestressing force $T_{\text{opt}}$ obtained with crossarm length ratio $\gamma$ varying.

| Case | $\gamma$ | $P_1^{\text{C}}$ (kN) | $P_2^{\text{C}}$ (kN) | Critical mode | $P^{\text{C}}$ (kN) | $T_{\text{opt}}$ (kN) |
|---|---|---|---|---|---|---|
| G1 | 0.5 | 84.05 | 74.11 | 2 | 74.11 | 1.85 |
| G2 | 0.6 | 98.94 | 82.55 | 2 | 82.55 | 2.09 |
| G3 | 0.7 | 104.93 | 91.12 | 2 | 91.12 | 2.32 |
| G4 | 0.8 | 102.02 | 99.87 | 2 | 99.87 | 2.56 |
| G5 | 0.9 | 94.57 | 108.73 | 1 | 94.57 | 2.44 |
| G6 | 1.0 | 86.08 | 117.51 | 1 | 86.08 | 2.22 |

*3.2. Levels of initial prestressing force*

Post-buckling analysis is also conducted within ABAQUS with the consideration of initial imperfections and the prestress within the eight stay components defined in Figure 3(a). As described in Figure 5, which indicates that when a very small prestress is applied to the stays, owing to the axial shortening of the main column, all the stay components go slack before the Euler load is reached. In this particular case, the system is effectively identical to the unstayed column with the buckling load being the Euler load. In order to mimic the behaviour of the perfect case, a very small column initial out-of-straightness, $\delta = 1/10000$, is used to represent a nearly perfect system. A small prestress, where $\sigma_{\rm s} = 5$ N/mm$^2$, such that the stayed column resides within Zone 1, is applied for the case with the stay diameter, the column aspect ratio and the crossarm length ratio being $\phi_{\rm s} = 4.8$ mm, $2\alpha_{\rm m} = 0.2$ and $\gamma = 0.8$ respectively.

Figure 10, shows the equilibrium paths of the stay component stresses $\sigma_{\rm s}$ and the column axial load $P$ versus the column mid-span lateral displacement $\delta_{\rm m}$ simultaneously for the nonlinear buckling response. It can be seen that initially the stresses in all eight stay components drop dramatically from 5 N/mm$^2$ to approximately 0.7 N/mm$^2$ and the axial force in the column increases from zero to approximately 3 kN with the mid-span deflection remaining at almost zero. This indicates that at the very early loading stage, the axial compression of the column is dominant while the lateral deflection is negligible.

Along with the increase of the external axial load, the mid-span deflection of the column begins to increase gradually, which means that the lateral deflection of the column becomes increasingly important. However, it can be seen that the stresses in all eight stay components are still decreasing, indicating that the axial shortening of the column still dominates. This is the stage when all stay components are de-stressing until a temporary buckling load, which is practically equal to the Euler load of the unstayed main column element, is observed while only one of the stay components is marginally active. However, this approximate Euler load does not become the eventual ultimate load of the stayed column system, as predicted for the theoretically perfect case. While the mid-span deflection of the column increases further, stay component 3, which is on the convex side of the slightly asymmetric column, almost goes slack but subsequently its tensile force begins to increase gradually. This is followed by the stay 2 component reactivating from slack and the stayed column axial force begins to increase at a larger rate with $\delta_{\rm m}$.

As expected, along with the increase of the column mid-span deflection, the stay components on the convex side of the column regain their tensile force one by one. Therefore the axial force in the column also keeps increasing until the actual load carrying capacity is eventually reached. It can be seen that owing to the mechanism of de-stressing and re-stressing of the stay components, the Euler load is not in fact practically applicable for the imperfect system within Zone 1. Even with such a small imperfection that aims to mimic the perfect case, the actual Euler instability can only be observed for a very small deformation range while the effect of the stay components re-stressing dominates the behaviour and the axial load increases. Indeed, in more realistic cases, for example when the initial out-of-straightness $\delta$ of the column is 1/300, which is the EC3 design value for hot rolled sections [33], the lateral deflection of the column dominates over the axial compression

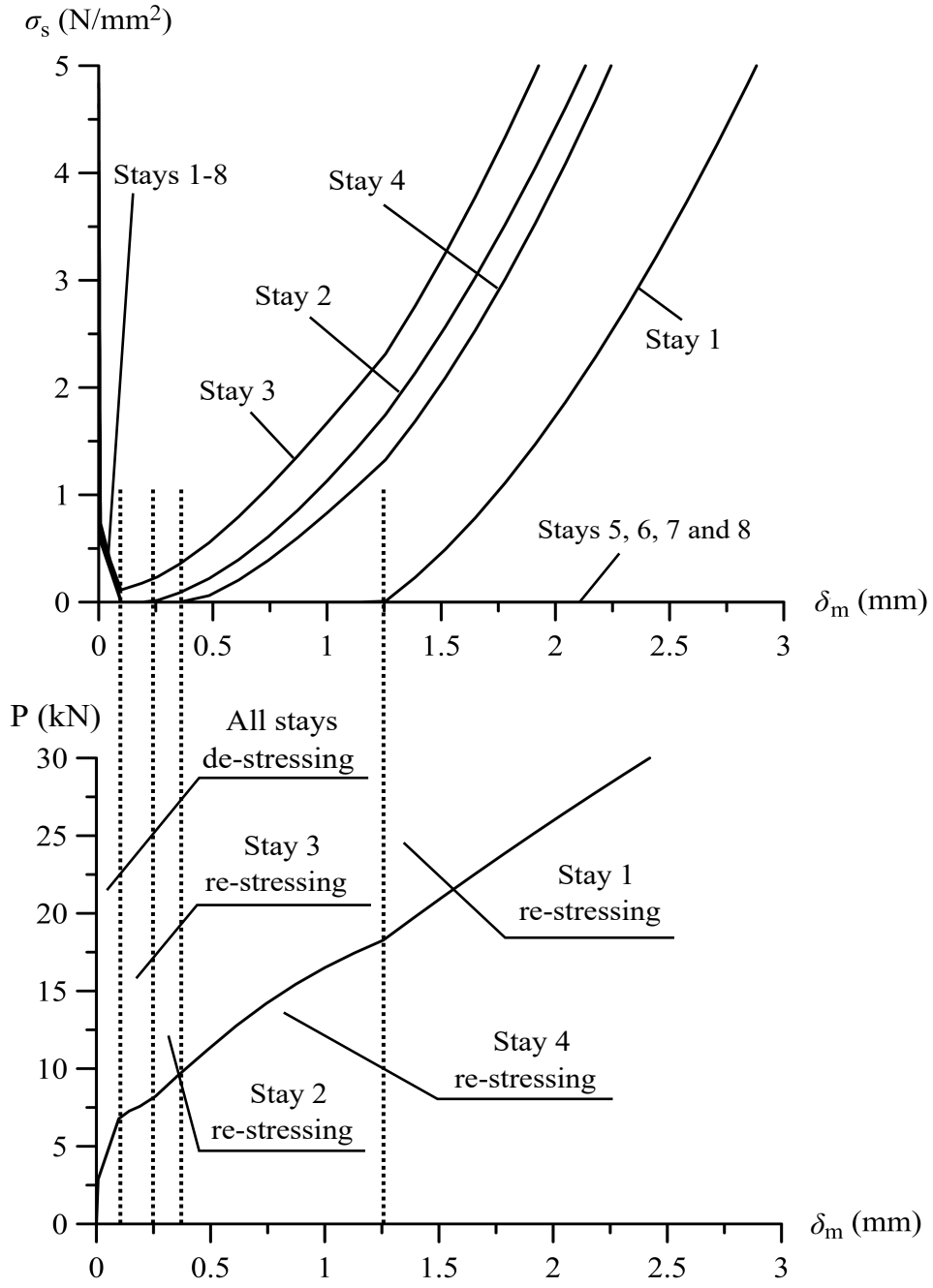


Figure 10: Equilibrium paths of the stresses $\sigma_s$ within the eight stay components defined in Figure 3(a) and the column axial load $P$ versus the column mid-span lateral displacement $\delta_m$ for interactive buckling when $\sigma_s = 5$ N/mm$^2$ initially. In this case, $\phi_s = 4.8$ mm, $2\alpha_m = 0.2$ and $\gamma = 0.8$.

much earlier than the nearly perfect case presented above. None of the stay components on the convex side of the column go slack; the stresses in these stay components decrease by a small amount at the very early loading stage and immediately begin to increase when the previously slack stay components reactivate. Therefore, the loss of stiffness at, or near the Euler buckling load, cannot be practically observed in these more realistic cases. Similarly, for Zone 2 prestress levels, even if a nearly perfect case is investigated, owing to the fact that the lateral deflection is sufficiently large to dominate over the axial displacement of the column, the situation where the prestress in the stay disappears at the instant when the column buckles cannot be practically observed either. The stay components on the convex side of the column would already be in the re-stressing stage before the buckling load is reached. Therefore, the prediction of the relationship between the Zone 2 initial prestressing force and the buckling load is also not suitable for the imperfect cases.

Figure 11 shows the comparison of the relationships of the load carrying capacity and

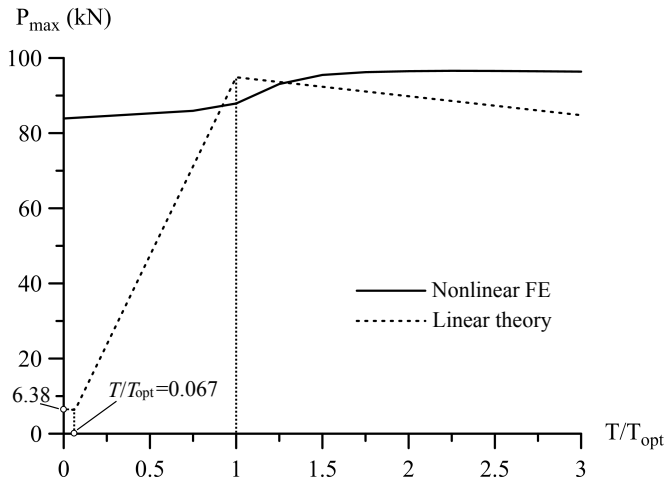


Figure 11: Comparison of relationships of load carrying capacity versus initial prestressing force from the nonlinear FE and the linear theoretical models for the triple-bay stayed column where $\phi_{\mathrm{s}} = 4.8$ mm, $2\alpha_{\mathrm{m}} = 0.2$ and $\gamma = 0.8$. Note that the FE results show that prestress levels where $T/T_{\mathrm{opt}} > 1$ would be advantageous in terms of ultimate capacity.

the initial prestressing force from the FE and the linear theoretical models. It can be seen that there are highly significant differences when comparing Zones 1 and 2 between the FE and the theoretical results from the linear model, even though the initial out-of-straightness of the column $\delta = 1/10000$ is adopted. The FE relationship is qualitatively in accordance with experimental data obtained for the single-bay prestressed stayed column [14]. It can also be seen that increasing the initial prestressing force from $T_{\mathrm{opt}}$ could still provide benefit in terms of the load carrying capacity, which was also observed previously [15, 26]. Therefore, initial prestressing forces larger than or equal to $T_{\mathrm{opt}}$ are investigated to find the actual optimal initial prestressing force of the triple-bay prestressed stayed column.

*3.3. Ultimate load carrying capacities with varying initial prestress*

Nine different levels of the initial prestressing force, with an increment of $0.25T_{\text{opt}}$ ranging from $T_{\text{opt}}$ to $3T_{\text{opt}}$, are studied for each case while focusing on the efficiency indicators for the column $\eta_{\text{c}}$ and for the stays $\eta_{\text{s}}$. Therefore, 162 separate cases in total are studied.

*3.3.1. Stay diameter $\phi_{\text{s}}$ variation*

Figure 12 shows the relationships of the maximum load capacities $P_{\text{max}}$ versus the

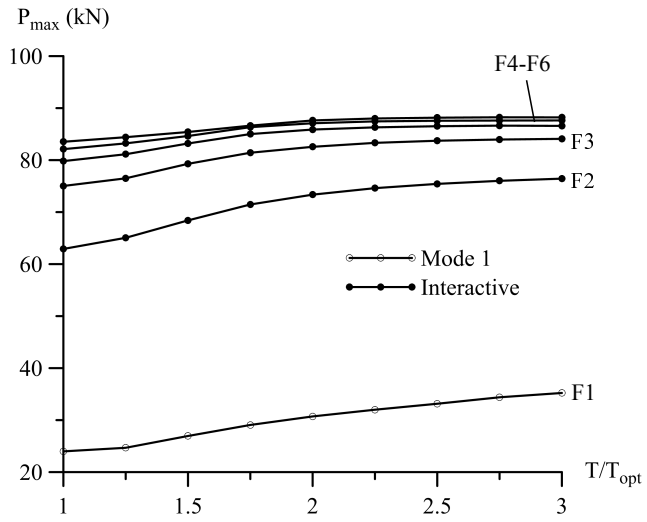


Figure 12: Relationships of maximum load capacities $P_{\text{max}}$ versus normalized initial prestressing forces in the stays $T/T_{\text{opt}}$ with the stay diameter $\phi_{\text{s}}$ varying (cases F1–F6).

normalized initial prestressing forces in the stays $T/T_{\text{opt}}$ with the stay diameter $\phi_{\text{s}}$ varying. Owing to the very small stay diameter (1.6 mm) adopted in case F1, its load carrying capacities are much lower than the other cases. It can be seen that for all six cases, increasing the initial prestressing force from $T_{\text{opt}}$ provides additional load carrying capacity. However, for cases F2–F6, this benefit is not obvious once the initial prestressing force reaches beyond approximately $2T_{\text{opt}}$. It can also be seen that the load carrying capacity stops rising if the initial prestressing force is increased further for cases F3–F6.

Figure 13 shows the relationships of the required column resistance $f_{\text{y,req}}$ and the corresponding efficiency indicator $\eta_{\text{c}}$ versus the normalized initial prestressing forces in the stays $T/T_{\text{opt}}$ with the stay diameter $\phi_{\text{s}}$ varying at the point of maximum load. As shown in Figure 13(a), the required resistance of the column for case F1 is basically constant, while for cases F2–F6 the required resistance decreases first and then increases once the initial prestressing force reaches $1.5T_{\text{opt}}$ (F2–F5) or $1.75T_{\text{opt}}$ (F6). It can also be seen that if the yield stress of the column is initially set to a nominal 355 N/mm$^2$, the required resistance for cases with large stay diameters requires a higher grade of steel for the column, which would put it in the range of what is popularly known as 'high strength steel' (or HSS) [35],

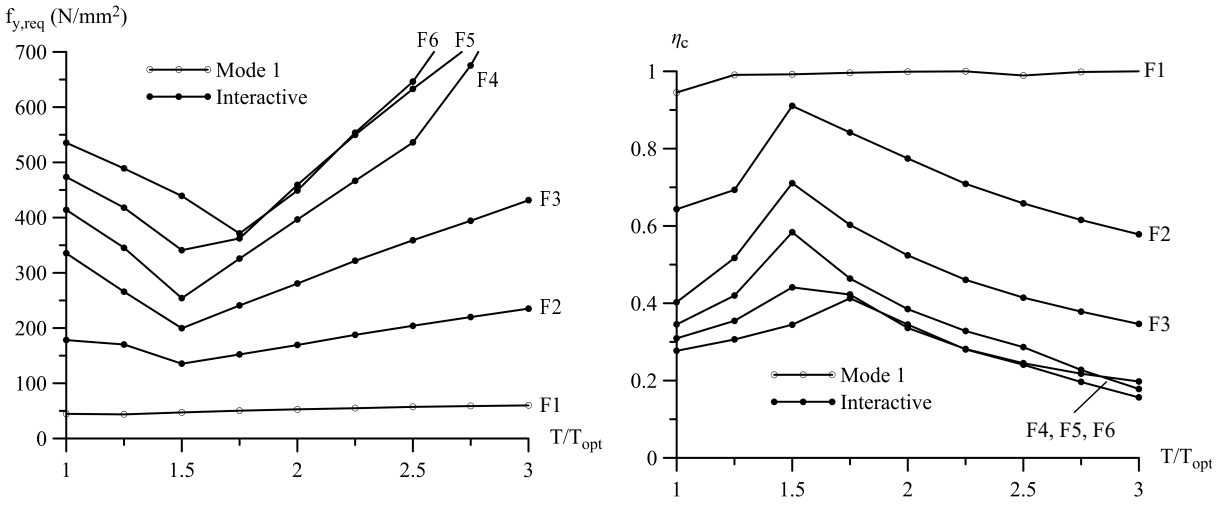


(a) Required column resistance $f_{\mathrm{y,req}}$

(b) Efficiency indicator $\eta_{\mathrm{c}}$ for the column

Figure 13: Relationships of required column resistance $f_{\mathrm{y,req}}$ and corresponding efficiency indicator $\eta_{\mathrm{c}}$ versus normalized initial prestressing forces in the stays $T/T_{\mathrm{opt}}$ with the stay diameter $\phi_{\mathrm{s}}$ varying (cases F1–F6).

where $f_{\mathrm{y}} \geqslant 460$ N/mm$^2$. This is particularly obvious when adopting a very small or a very large prestress. As stated earlier, higher values of the efficiency indicator for the column are preferred. It can be seen in Figure 13(b) that for cases F2–F6, the highest indicator values are found when the initial prestressing force $T = 1.5T_{\mathrm{opt}}$ (F2–F5) or $T = 1.75T_{\mathrm{opt}}$ (F6). It is very important to note that this is just the range where the required column resistance is found to be a minimum.

Similarly, Figure 14 shows the relationships of the required stay resistance $f_{\mathrm{s,req}}$ and the corresponding efficiency indicator $\eta_{\mathrm{s}}$ versus the normalized initial prestressing forces in the stays $T/T_{\mathrm{opt}}$ with the stay diameter $\phi_{\mathrm{s}}$ varying at the point of maximum load. Again, the best values of the efficiency indicator are found mostly when the initial prestressing force $T = 1.5T_{\mathrm{opt}}$ and $1.75T_{\mathrm{opt}}$, as shown in Figure 14(b). This range is in accordance with the finding obtained in the cases studying the efficiency indicator for the column $\eta_{\mathrm{c}}$. The actual optimal prestress selected on the basis of the efficiency indicators of the column and the stays are presented in Table 7.

*3.3.2. Column aspect ratio $2\alpha_{\mathrm{m}}$ variation*

Figure 15 shows the relationships of the maximum load capacities $P_{\mathrm{max}}$ versus the normalized initial prestressing forces in the stays $T/T_{\mathrm{opt}}$ with the column aspect ratio $2\alpha_{\mathrm{m}}$ varying. It can be seen again that additional load carrying capacities can be obtained by increasing the initial prestressing force from $T_{\mathrm{opt}}$. However, the load carrying capacity trends again become rather flat when the initial prestressing force reaches approximately $2T_{\mathrm{opt}}$, indicating that not too much additional benefit is obtained by increasing the initial prestressing force further. It can also be seen that cases a3–a6 provide higher load carrying capacities.

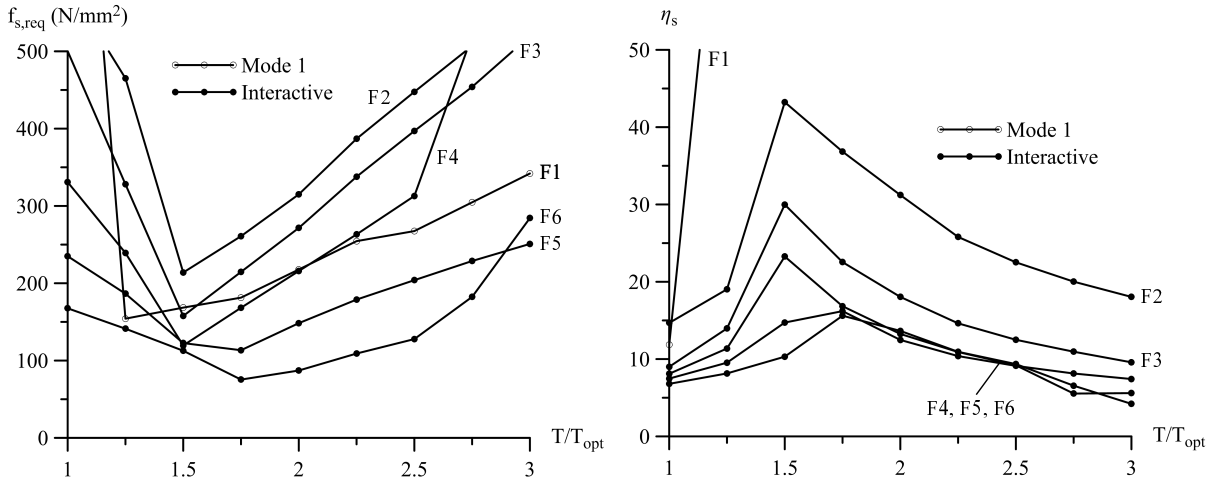


(a) Required stay resistance $f_{\mathrm{s,req}}$ (b) Efficiency indicator $\eta_{\mathrm{s}}$ for the stays

Figure 14: Relationships of required stay resistance $f_{\mathrm{s,req}}$ and corresponding efficiency indicator $\eta_{\mathrm{s}}$ versus normalized initial prestressing forces in the stays $T/T_{\mathrm{opt}}$ with the stay diameter $\phi_{\mathrm{s}}$ varying (cases F1–F6).

Table 7: Actual optimal initial prestressing force obtained from the column indicator $T_{\mathrm{opt,c}}$ and from the stay indicator $T_{\mathrm{opt,s}}$ with the stay diameter $\phi_{\mathrm{s}}$ varying.

| Case | $\phi_{\mathrm{s}}$ (mm) | $T_{\mathrm{opt,c}}/T_{\mathrm{opt}}$ | $T_{\mathrm{opt,s}}/T_{\mathrm{opt}}$ | Buckling mode |
|---|---|---|---|---|
| F1 | 1.6 | – | – | Mode 1 |
| F2 | 3.2 | 1.50 | 1.50 | Interactive |
| F3 | 4.8 | 1.50 | 1.50 | Interactive |
| F4 | 6.4 | 1.50 | 1.50 | Interactive |
| F5 | 8.0 | 1.50 | 1.75 | Interactive |
| F6 | 10.0 | 1.75 | 1.75 | Interactive |

Figure 16 shows the relationships of the required column resistance $f_{\mathrm{y,req}}$ and the corresponding efficiency indicator $\eta_{\mathrm{c}}$ versus the normalized initial prestressing forces in the stays $T/T_{\mathrm{opt}}$ with the column aspect ratio $2\alpha_{\mathrm{m}}$ varying at the point of maximum load. It can be seen in Figure 16 that for cases a1 and a2, the respective required column resistances increase with the initial prestressing force, with the latter possessing a higher rate of increase with $T/T_{\mathrm{opt}}$. For cases a3–a6, the required column resistances decrease first and then increase. The minimum required column resistance can be found when $T = 1.5T_{\mathrm{opt}}$. Note that for larger values of the column aspect ratio, such as a4–a6, the required respective column resistances, only within the range from $1.25T_{\mathrm{opt}}$ to $2.5T_{\mathrm{opt}}$, are less than the assumed column yield stress (355 N/mm$^2$); otherwise higher strength steels, including those classified specifically as HSS, would tend to be required.

Similarly, Figure 17 shows the relationships of the required stay resistance $f_{\mathrm{s,req}}$ and the corresponding efficiency indicator $\eta_{\mathrm{s}}$ versus the normalized initial prestressing forces in the stays $T/T_{\mathrm{opt}}$ with the column aspect ratio $2\alpha_{\mathrm{m}}$ varying at the point of maximum

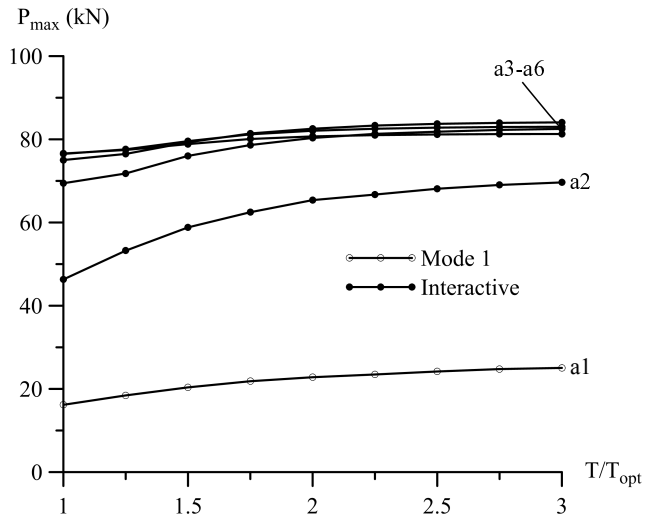


Figure 15: Relationships of maximum load capacities $P_{\max}$ versus normalized initial prestressing forces in the stays $T/T_{\text{opt}}$ with the column aspect ratio $2\alpha_{\text{m}}$ varying (cases a1–a6).

load. As shown in Figure 17(a), the minimum required stay resistances can be found when $T = 1.5T_{\text{opt}}$ for cases a3–a6, while they are $1.25T_{\text{opt}}$ for case a1 and $T_{\text{opt}}$ for case a2. Again, as can be seen in Figure 17(b), the preferred efficiency indicator values are mostly found when $T = 1.5T_{\text{opt}}$. The actual optimal prestress selected on the basis of the efficiency indicators of the column and the stays are presented in Table 8.

Table 8: Actual optimal initial prestressing force obtained from the column indicator $T_{\text{opt,c}}$ and from the stay indicator $T_{\text{opt,s}}$ with the column aspect ratio $2\alpha_{\text{m}}$ varying.

| Case | $2\alpha_{\text{m}}$ | $T_{\text{opt,c}}/T_{\text{opt}}$ | $T_{\text{opt,s}}/T_{\text{opt}}$ | Buckling mode |
|---|---|---|---|---|
| a1 | 0.05 | 1.50 | 1.25 | Mode 1 |
| a2 | 0.10 | 1.00 | 1.00 | Interactive |
| a3 | 0.15 | 1.50 | 1.50 | Interactive |
| a4 | 0.20 | 1.50 | 1.50 | Interactive |
| a5 | 0.25 | 1.50 | 1.50 | Interactive |
| a6 | 0.30 | 1.50 | 1.50 | Interactive |

*3.3.3. Crossarm length ratio $\gamma$ variation*

Figure 18 shows the relationships of the maximum load capacities $P_{\max}$ versus the normalized initial prestressing forces in the stays $T/T_{\text{opt}}$ with the crossarm length ratio $\gamma$ varying. It can be seen that the additional load carrying capacities can be obtained by increasing the initial prestressing force from $T_{\text{opt}}$, but this benefit is, again, not so obvious when the initial prestressing force is set to a level significantly above $2T_{\text{opt}}$. It can also be seen that increasing $\gamma$ values from 0.5 to 0.8 significantly increases the load carrying

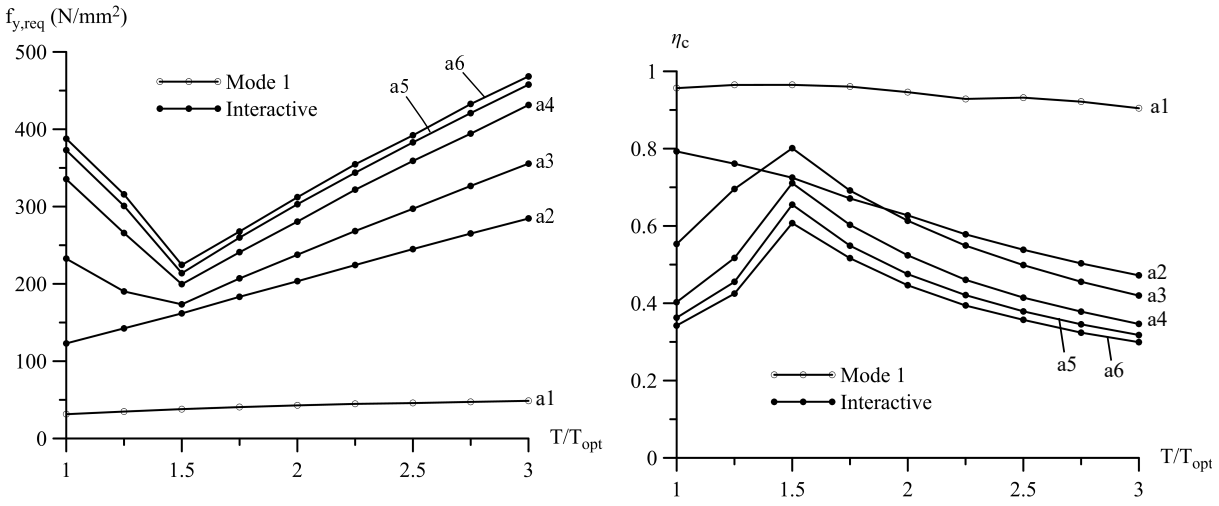


(a) Required column resistance $f_{\mathrm{y,req}}$

(b) Efficiency indicator $\eta_{\mathrm{c}}$ for the column

Figure 16: Relationships of required column resistance $f_{\mathrm{y,req}}$ and corresponding efficiency indicator $\eta_{\mathrm{c}}$ versus normalized initial prestressing forces in the stays $T/T_{\mathrm{opt}}$ with the column aspect ratio $2\alpha_{\mathrm{m}}$ varying (cases a1–a6).

capacity of the column. However, when $\gamma$ is increased further to 0.9 and 1.0, a decrease in the load carrying capacity can be observed when the initial prestressing force is larger than $1.75T_{\mathrm{opt}}$, owing to the fact that the middle crossarm becomes inherently less effective.

Figure 19 shows the relationships of the required column resistance $f_{\mathrm{y,req}}$ and the corresponding efficiency indicator $\eta_{\mathrm{c}}$ versus the normalized initial prestressing forces in the stays $T/T_{\mathrm{opt}}$ with the crossarm length ratio $\gamma$ varying at the point of maximum load. As shown in Figure 19(a), the required column resistances decrease first and then increase with the initial prestressing force. The lowest required column resistance can be found when $T = 1.5T_{\mathrm{opt}}$ for cases G2–G6 and $T = 1.75T_{\mathrm{opt}}$ for case G1. As expected, it can be seen in Figure 19(b) that the preferred efficiency indicator values of the column can be mostly found when $T = 1.5T_{\mathrm{opt}}$.

Similarly, Figure 20 shows the relationships of the required stay resistance $f_{\mathrm{s,req}}$ and the corresponding efficiency indicator $\eta_{\mathrm{s}}$ versus the normalized initial prestressing forces in the stays $T/T_{\mathrm{opt}}$ with the crossarm length ratio $\gamma$ varying at the point of maximum load. It can be seen in Figure 20(a) that the required stay resistances decrease initially and then increase with the initial prestressing force. The lowest required stay resistance can be found when the initial prestressing force is $1.5T_{\mathrm{opt}}$ and $1.75T_{\mathrm{opt}}$. As shown in Figure 20(b), the highest values of the efficiency indicator for the stays can be found when the initial prestressing force ranges from $1.5T_{\mathrm{opt}}$ to $1.75T_{\mathrm{opt}}$. Therefore, the actual optimal prestress may be selected on the basis of the efficiency indicators of the column and the stays are presented in Table 9.

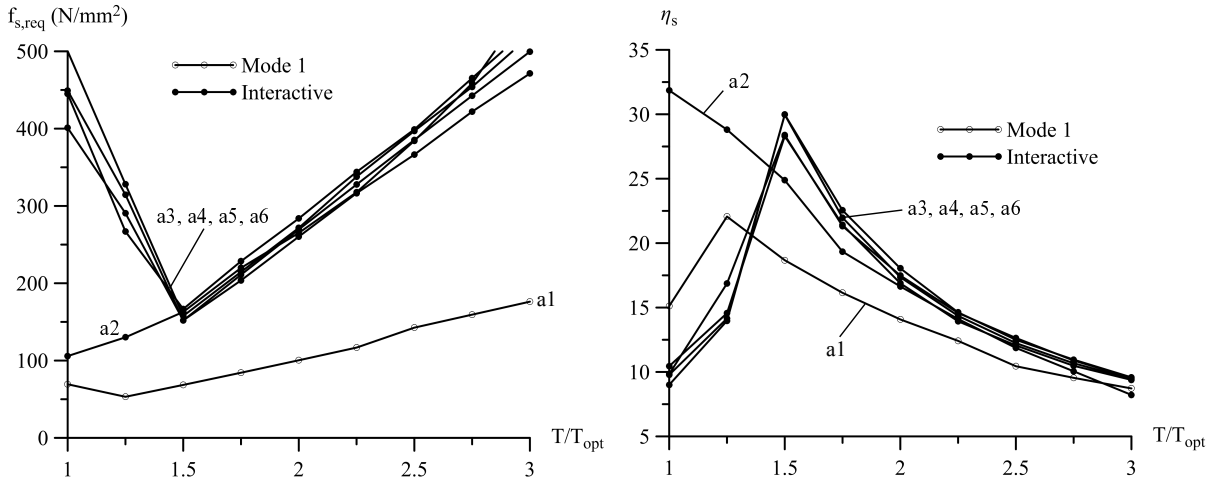


(a) Required stay resistance $f_{\mathrm{s,req}}$ (b) Efficiency indicator $\eta_{\mathrm{s}}$ for the stays

Figure 17: Relationships of required stay resistance $f_{\mathrm{s,req}}$ and corresponding efficiency indicator $\eta_{\mathrm{s}}$ versus normalized initial prestressing forces in the stays $T/T_{\mathrm{opt}}$ with the column aspect ratio $2\alpha_{\mathrm{m}}$ varying (cases a1–a6).

Table 9: Actual optimal initial prestressing force obtained from the column indicator $T_{\mathrm{opt,c}}$ and from the stay indicator $T_{\mathrm{opt,s}}$ with the crossarm length ratio $\gamma$ varying.

| Case | $\gamma$ | $T_{\mathrm{opt,c}}/T_{\mathrm{opt}}$ | $T_{\mathrm{opt,s}}/T_{\mathrm{opt}}$ | Buckling mode |
|---|---|---|---|---|
| G1 | 0.5 | 1.75 | 1.75 | Interactive |
| G2 | 0.6 | 1.50 | 1.75 | Interactive |
| G3 | 0.7 | 1.50 | 1.50 | Interactive |
| G4 | 0.8 | 1.50 | 1.50 | Interactive |
| G5 | 0.9 | 1.50 | 1.50 | Mode 1 |
| G6 | 1.0 | 1.50 | 1.50 | Mode 1 |

### *3.4. Further parametric studies*

In the current section, the actual optimal initial prestressing force is investigated over a wider range of the geometric configurations. It can be seen in Figure 18 that the crossarm length ratio $\gamma = 0.8$ provides the highest load carrying capacity, which indicates that both the middle and the edge crossarms are sufficiently effective in this ratio. Therefore, a series of cases where the stay diameter and the column aspect ratio are varied simultaneously with the crossarm length ratio $\gamma$ being fixed to 0.8 are studied. Nine different levels of initial prestressing force ranging from $T_{\mathrm{opt}}$ to $3T_{\mathrm{opt}}$ with an increment of $0.25T_{\mathrm{opt}}$ are adopted for six different stay diameters and six different column aspect ratios. In total, a further 324 cases are investigated currently.

The buckling analysis of the 36 cases with the different stay diameters and the column aspect ratios is first conducted. With the obtained buckling loads, the theoretical optimal prestress $T_{\mathrm{opt}}$ can be calculated for each case. Similar to the aforementioned method, non-

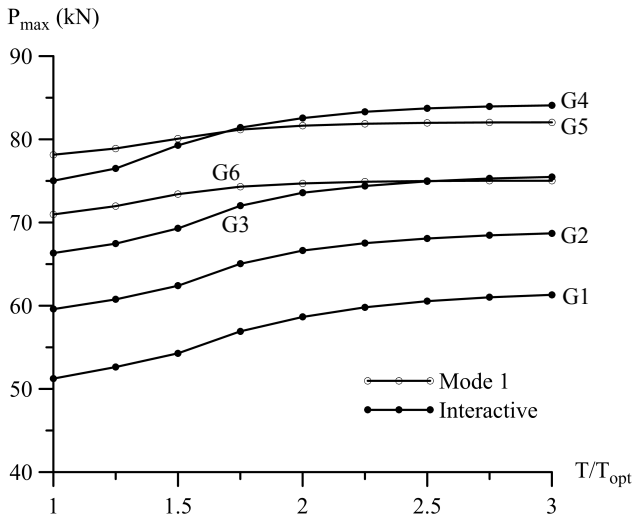


Figure 18: Relationships of maximum load capacities $P_{\max}$ versus normalized initial prestressing forces in the stays $T/T_{\text{opt}}$ with the crossarm length ratio $\gamma$ varying (cases G1–G6).

linear post-buckling analysis is then conducted with the adoption of nine different levels of initial prestressing force and corresponding imperfection profiles. The results of the column load carrying capacity and the required resistances of the column and the stays can then be obtained. The values of the two efficiency indicators can therefore be calculated. Tables 10 and 11 summarize the levels of the actual optimal initial prestressing force obtained

Table 10: Actual optimal initial prestressing force based on the efficiency indicator of the column $\eta_{\text{c}}$ with the stay diameter $\phi_{\text{s}}$ and the column aspect ratio $2\alpha_{\text{m}}$ varying simultaneously while $\gamma = 0.8$.

| Case | a1 | a2 | a3 | a4 | a5 | a6 |
|---|---|---|---|---|---|---|
| F1 | – | – | – | – | – | $1.25T_{\text{opt}}$ |
| F2 | – | – | – | $1.5T_{\text{opt}}$ | $1.5T_{\text{opt}}$ | $1.5T_{\text{opt}}$ |
| F3 | – | – | $1.5T_{\text{opt}}$ | $1.5T_{\text{opt}}$ | $1.5T_{\text{opt}}$ | $1.5T_{\text{opt}}$ |
| F4 | – | $1.25T_{\text{opt}}$ | $1.5T_{\text{opt}}$ | $1.5T_{\text{opt}}$ | $1.5T_{\text{opt}}$ | $1.5T_{\text{opt}}$ |
| F5 | $1.0T_{\text{opt}}$* | $1.5T_{\text{opt}}$ | $1.5T_{\text{opt}}$ | $1.5T_{\text{opt}}$ | $1.5T_{\text{opt}}$ | $1.5T_{\text{opt}}$ |
| F6 | $1.0T_{\text{opt}}$ | $1.75T_{\text{opt}}$ | $1.75T_{\text{opt}}$ | $1.75T_{\text{opt}}$ | $1.75T_{\text{opt}}$ | $1.75T_{\text{opt}}$ |

based on the efficiency indicators of the column $\eta_{\text{c}}$ and the stays $\eta_{\text{s}}$ respectively. Note that the '*' symbol after the force value indicates that Mode 1 governs the respective post-buckling behaviour, while the others are governed by nonlinear interactive post-buckling behaviour. It can be seen that for most of the cases in both tables, the actual optimal initial prestressing force is $1.5T_{\text{opt}}$, while for cases with larger stay diameters the optimal initial prestressing force becomes $1.75T_{\text{opt}}$. This is significantly different from the results for the single-bay prestressed stay column, where the actual optimal initial prestressing force mostly ranged between $2T_{\text{opt}}$ and $3T_{\text{opt}}$ [20]. Note that the actual optimal prestress

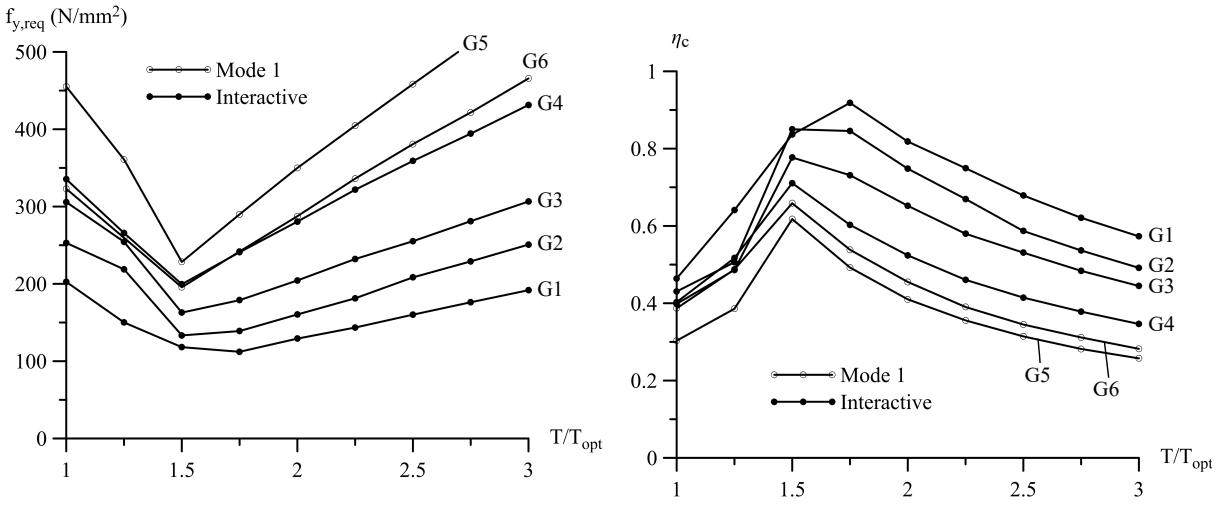


(a) Required column resistance $f_{\mathrm{y,req}}$

(b) Efficiency indicator $\eta_{\mathrm{c}}$ for the column

Figure 19: Relationships of required column resistance $f_{\mathrm{y,req}}$ and corresponding efficiency indicator $\eta_{\mathrm{c}}$ versus normalized initial prestressing forces in the stays $T/T_{\mathrm{opt}}$ with the crossarm length ratio $\gamma$ varying (cases G1–G6).

Table 11: Similar to Table 10, the optimal initial prestressing force based on the efficiency indicator of the stay $\eta_{\mathrm{s}}$ again while $\gamma = 0.8$.

| Case | a1 | a2 | a3 | a4 | a5 | a6 |
|---|---|---|---|---|---|---|
| F1 | – | – | – | – | – | – |
| F2 | – | – | – | $1.5T_{\mathrm{opt}}$ | $1.5T_{\mathrm{opt}}$ | $1.5T_{\mathrm{opt}}$ |
| F3 | – | – | $1.5T_{\mathrm{opt}}$ | $1.5T_{\mathrm{opt}}$ | $1.5T_{\mathrm{opt}}$ | $1.5T_{\mathrm{opt}}$ |
| F4 | – | $1.5T_{\mathrm{opt}}$ | $1.5T_{\mathrm{opt}}$ | $1.5T_{\mathrm{opt}}$ | $1.5T_{\mathrm{opt}}$ | $1.5T_{\mathrm{opt}}$ |
| F5 | $1.0T_{\mathrm{opt}}$* | $1.5T_{\mathrm{opt}}$ | $1.75T_{\mathrm{opt}}$ | $1.75T_{\mathrm{opt}}$ | $1.5T_{\mathrm{opt}}$ | $1.5T_{\mathrm{opt}}$ |
| F6 | $1.5T_{\mathrm{opt}}$ | $1.75T_{\mathrm{opt}}$ | $1.75T_{\mathrm{opt}}$ | $1.75T_{\mathrm{opt}}$ | $1.75T_{\mathrm{opt}}$ | $1.75T_{\mathrm{opt}}$ |

in terms of the efficiency indicators cannot satisfactorily be found for configurations with both a very small stay diameter and a small column aspect ratio. This is not entirely surprising nor problematic since in those configurations the stayed column would, in any case, approximately behave as an unstayed column. Nevertheless, a suitable prestress may still be selected by checking the column load carrying capacity and the required resistances of the column and the stays when designing structures with the configurations within those ranges.

## 4. Concluding remarks

A nonlinear FE model has been developed to investigate the actual optimal prestress for the triple-bay prestressed stayed column the objective of which was to maximize the overall system efficiency. It was shown that although extra load carrying capacity can be obtained by increasing the initial prestressing force from the linearly obtained benchmark

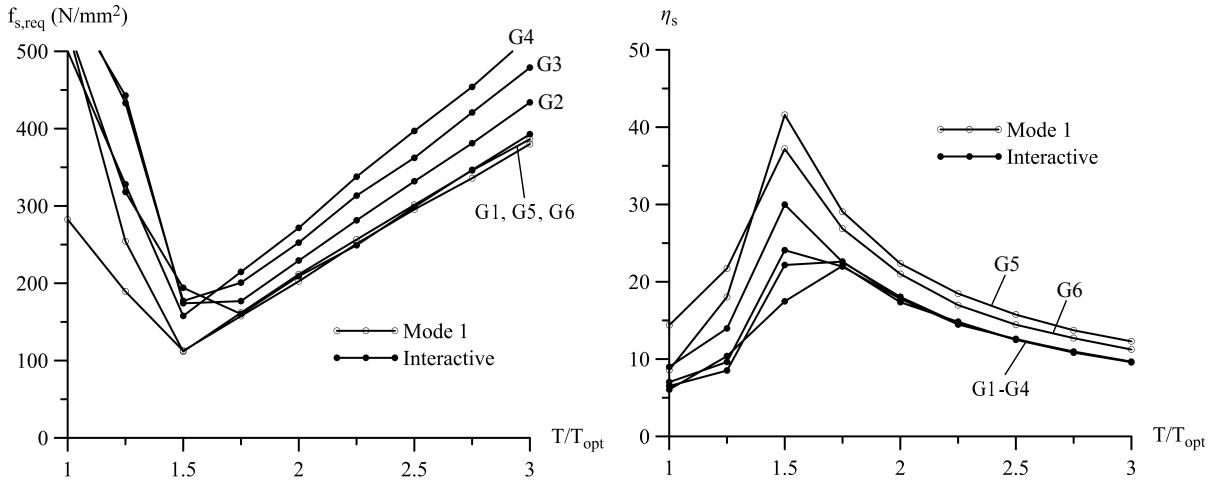


(a) Required stay resistance $f_{\mathrm{s,req}}$

(b) Efficiency indicator $\eta_{\mathrm{s}}$ for the stays

Figure 20: Relationships of required stay resistance $f_{\mathrm{s,req}}$ and corresponding efficiency indicator $\eta_{\mathrm{s}}$ versus normalized initial prestressing forces in the stays $T/T_{\mathrm{opt}}$ with the crossarm length ratio $\gamma$ varying (cases G1–G6).

level $T_{\mathrm{opt}}$, introducing excessively large prestress levels can decrease the ultimate load carrying capacity of the column. In addition, once the column begins to deflect laterally, the stress within the stays on the convex side of the column may exceed the material strength. Therefore, nominating an optimal prestress by only considering the load carrying capacity is neither necessarily efficient nor safe. As a result, a pair of efficiency indicators, which take into account the load carrying capacity together with the required resistances of the column and the stays simultaneously, are used to guide the determination of the actual optimal initial prestress.

The actual optimal initial prestress values were presented while varying the stay diameter, the column aspect ratio and the crossarm ratio while other parameters were fixed. The corresponding values were also presented for cases where the stay diameter and the column aspect ratio were varied simultaneously, while the crossarm ratio was fixed to its most advantageous value. It was demonstrated that in most cases, for the chosen example configuration, the actual optimal initial prestressing force is $1.5T_{\mathrm{opt}}$, while for cases with larger stay diameters the initial force level may become $1.75T_{\mathrm{opt}}$, which is considerably smaller than the levels found for the single-bay column case of similar properties. It is worth noting that the determination of the optimal initial prestressing force is based on the preferred values of the aforementioned efficiency indicators that also reflect the general cost effectiveness. So long as the required resistances of the column and the stays are within the elastic range and are examined with due care, the load carrying capacity of the main column element may also be the single factor in determining the actual optimal prestress. This would be particularly important if a high load carrying capacity is of paramount importance for a specific column arrangement.

Although a reasonably limited set of numerical cases were presented, the current work

provides a rational methodology for optimising the prestress within a given stayed column configuration. In future work, more geometric parameters of the structure could be varied, such as the position and size of the intermediate crossarms along the length and the main column slenderness. Moreover, the inclusion of additional stay cables may also improve the performance and this is currently being investigated. Experimental studies are also desirable to validate the observations from the current modelling. In addition, the actual cost of different grades of steel for the column and the stays could also be included within the cost effectiveness calculation explicitly. Hence, enhanced efficiency indicators that include costs of materials and fabrication would therefore provide more precise optimal initial prestress levels but, again, this consideration is left for future studies.

## References


[1] S. A. L. Andrade, P. C. G. d. S. Vellasco, J. G. S. Silva, Concepcao e projecto estrutural do palco principal do Rock in Rio III, Construcao Magazine 6 (2003) 4–11.

[2] S. A. L. Andrade, P. C. G. d. S. Vellasco, J. G. S. Silva, Sistema construtivo e montagem estrutural do palco Principal do Rock in Rio III, Construcao Magazine 7 (2003) 30–35.

[3] K. H. Chu, S. S. Berge, Analysis and design of struts with tension ties, ASCE Journal of the Structural Division 89 (1963) 127–163.

[4] A. H. Chilver, Coupled modes of elastic buckling, Journal of the Mechanics and Physics of Solids 15 (1967) 15–28.

[5] H. R. Mauch, Optimum design of columns supported by tension ties, ASCE Journal of Structural Engineering 93 (3) (1967) 201–220.

[6] R. J. Smith, J. S. Ellis, G. T. McCaffrey, Buckling of a single-crossarm stayed column, ASCE Journal of the Structural Division 101 (1) (1975) 249–268.

[7] M. C. Temple, Buckling of stayed columns, ASCE Journal of the Structural Division 103 (4) (1977) 839–851.

[8] E. Belenya, Prestressed load-bearing metal structures, Moscow: Mir Publishers, 1977.

[9] W. P. Howson, F. W. Williams, A parametric study of the initial buckling of stayed columns, Proceedings of the Institution of Civil Engineers 69 (1980) 261–279.

[10] H. H. Hafez, M. C. Temple, J. S. Ellis, Pretensioning of single-crossarm stayed columns, ASCE Journal of the Structural Division 105 (2) (1979) 359–375.

[11] K. C. Wong, M. C. Temple, Stayed column with initial imperfection, ASCE Journal of the Structural Division 108 (1982) 1623–1640.

[12] M. C. Temple, M. V. Prakash, J. S. Ellis, Failure criteria for stayed columns, ASCE Journal of Structural Engineering 110 (1984) 2677–2689.

[13] D. Saito, M. A. Wadee, Post-buckling behaviour of prestressed steel stayed columns, Engineering Structures 30 (5) (2008) 1224–1239.

[14] A. I. Osofero, M. A. Wadee, L. Gardner, Experimental study of critical and post-buckling behaviour of prestressed steel stayed columns, Journal of Constructional Steel Research 79 (2012) 226–241.

[15] D. Saito, M. A. Wadee, Numerical studies of interactive buckling in prestressed steel stayed columns, Engineering Structures 31 (2) (2009) 432–443.

[16] M. A. Wadee, L. Gardner, T. A. Hunt, Buckling mode interaction in prestressed stayed columns, Proceedings of the Institution of Civil Engineers-Structures and Buildings 166 (2013) 403–412.

[17] M. Serra, A. Shahbazian, L. Simões da Silva, L. Marques, C. Rebelo, P. C. G. d. S. Vellasco, A full scale experimental study of prestressed stayed columns, Engineering Structures 100 (2015) 490–510.

[18] J. P. Martins, A. Shahbazian, L. Simões da Silva, C. Rebelo, R. Simões, Structural behaviour of prestressed stayed columns with single and double cross-arms using normal and high strength steel, Archives of Civil and Mechanical Engineering 16 (4) (2016) 618–633.

[19] J. Yu, M. A. Wadee, Mode interaction in triple-bay prestressed stayed columns, International Journal of Non-Linear Mechanics 88 (2017) 47–66.

[20] D. Saito, M. A. Wadee, Optimal prestressing and configuration of stayed columns, Proceedings of the Institution of Civil Engineers – Structures and Buildings 163 (5) (2010) 343–355.

[21] M. A. Wadee, L. Gardner, A. I. Osofero, Design of prestressed stayed columns, Journal of Constructional Steel Research 80 (2013) 287–298.

[22] E. A. Smith, Behavior of columns with pretensioned stays, ASCE Journal of Structural Engineering 111 (1985) 961–972.

[23] ABAQUS, Version 6.14 Documentaion, Dassault Systèmes Simulia Corp., Providence, RI, USA (2014).

[24] J. Yu, Nonlinear stability of prestressed stayed columns with multiple crossarm systems, Ph.D. thesis, Imperial College of Science, Technology and Medicine (2017).

[25] A. I. Osofero, M. A. Wadee, L. Gardner, Numerical studies on the buckling resistance of prestressed stayed columns, Advances in Structural Engineering 16 (2013) 487–498.

[26] J. Yu, M. A. Wadee, Numerical and analytical studies of prestressed stayed columns with multiple cross-arms, in: D. Camotim, P. B. Dinis, S. L. Chan, C. M. Wang, R. Gonçalves, N. Silverstre, C. Basaglia, A. Landesmann, R. Bebiano (Eds.), Proceedings of the Eighth International Conference on Advances in Steel Structures, 2015, paper number: 186.

[27] P. Li, M. A. Wadee, J. Yu, M. Wu, Stability of prestressed stayed steel columns with a three branch crossarm system, Journal of Constructional Steel Research 122 (2016) 274–291.

[28] C. Zschernack, M. A. Wadee, C. Völlmecke, Nonlinear buckling of fibre-reinforced unit cells of lattice materials, Composite Structures 136 (2016) 217–228.

[29] D. Saito, M. A. Wadee, Buckling behaviour of prestressed steel stayed columns with imperfections and stress limitation, Engineering Structures 31 (1) (2009) 1–15.

[30] M. A. Wadee, Effects of periodic and localized imperfections on struts on nonlinear foundations and compression sandwich panels, International Journal of Solids and Structures 37 (2000) 1191–1209.

[31] M. A. Wadee, L. A. P. Simões da Silva, Asymmetric secondary buckling in monosymmetric sandwich struts, ASME Journal of Applied Mechanics 72 (2005) 683–690.

[32] M. A. Wadee, M. Farsi, Imperfection sensitivity and geometric effects in stiffened plates susceptible to cellular buckling, Structures 3 (2015) 172–186.

[33] BS EN 1993-1-1, Eurocode 3: Design of steel structures - Part 1-1: General rules and rules for buildings, British Standards Institution (2005).

[34] N. S. Trahair, M. A. Bradford, D. A. Nethercot, L. Gardner, The behaviour and design of steel structures to EC3, 4th Edition, Taylor & Francis, London, 2008.

[35] J. Raoul, H.-P. Günther, Use and application of high-performance steels for steel structures, Vol. 8, IABSE, 2005.